Numerical study on oscillatory convection of cold water in a tall vertical enclosure

C.J. Ho and F.J. Tu
Department of Mechanical Engineering, National Cheng Kung University, Tainan, Taiwan, Republic of China

Received September 1998
Revised November 1998
Accepted December 1998

Keywords *Density, Natural convection, Numerical simulation, Water*

Abstract *The stability of two-dimensional natural convection of water near its density maximum (cold water) inside a vertical rectangular enclosure with an aspect ratio of eight is investigated via a series of direct numerical simulations. The simulations aim to clarify, under the influence of density inversion, the physical nature of the instability mechanism responsible for the laminar buoyancy-driven flow transition from a steady state to an oscillatory state in the enclosure filled with cold water. Two values of the density inversion parameter, θ_m= 0.4 and 0.5, where the density inversion of cold water may exert strong influence on the flow, are considered in the present study. The results show that the transition from steady state to periodically oscillatory convection arises in the cold-water-filled enclosure through a Hopf bifurcation. The oscillatory convection in the water-filled enclosure for both values of θ_m is found to feature an oscillatory multicellular structure within the contra-rotating bicellular flow regions. A traveling wave motion accordingly results along the maximum density contour, which demarcates the contra-rotating bicellular flows in the enclosure. For both cases the nature of transition into unsteadiness is found to be buoyancy-driven. The critical Rayleigh number for the bifurcation at θ_m = 0.4 is found to be markedly higher than that at θ_m = 0.5.*

Nomenclature

A = aspect ratio, H/W
b = exponent in the density equation
f^+ = frequency, Hz
f = dimensionless frequency, f^+W^2/α
g = gravitational acceleration, m/s^2
H = annulus height, m
k = thermal conductivity, $W/m \cdot K$
Nu = Nusselt number
Pr = Prandtl number, ν/α
Ra_H = Rayleigh number based on annulus height, $g \cdot rs\rho(\Delta T)^b H^3/(\nu\alpha)$
Ra_W = Rayleigh number based on gap width, $g \cdot rs\rho(\Delta T)^b W^3/(\nu\alpha)$
$rs\rho$ = coefficient in density equation
T = temperature, °C
ΔT = temperature difference between inner and outer wall, $(T_h - T_c)$, °C
t = time, s
u, ν = components of velocity, m/s
W = width, m
x^+, y^+ = Cartesian coordinates, m
x, y = dimensionless coordinates, x^+/W, y^+/W
α = thermal diffusivity,
θ = dimensionless temperature, $(T - T_c)/\Delta T$
θ_m = density inversion parameter, $(T_m - T_c)/\Delta T$
ν = kinematic viscosity, m^2/s
ρ = density, kg/m^3
τ = dimensionless time, $\alpha t/W^2$
$^+$ = stream function, m^3/s
ψ = dimensionless stream function, $^+/(\alpha W)$
ω^+ = vorticity, s^{-1}
ω = dimensionless vorticity, $\omega^+ W^2/\alpha$

Subscripts

cr = critical state
c = cold wall
h = hot wall
m = maximum density or periodically mean value

The authors gratefully acknowledge the financial support from National Science Council of ROC in Taiwan through Project No. NSC-84-2212-E006-013. The necessary computing facility and time are kindly provided by the National Center for High Performance Computing of NSC.

International Journal of Numerical Methods for Heat & Fluid Flow, Vol. 9 No. 4, 1999, pp. 487-508.

Introduction

Water and several liquid metals are known to feature an anomalous density-temperature relationship, the so-called density inversion phenomenon, having their maximum density at a temperature T_m above the freezing temperature. For water at sea-level atmospheric pressure is about 4°C. The density inversion phenomenon of water near 4°C (cold water) is known to provoke some peculiar behaviors of the buoyancy-driven convection flow and heat transfer in enclosure, such as multicellular flow structure and heat transfer extreme. Owing to the important role it plays in many technical and engineering applications, natural convection of cold water in a vertical rectangular enclosure has received considerable research attentions since the pioneering numerical work by Watson (1972). Representative works include Seki *et al.* (1978a,b), Inaba and Fukuda (1984a,b), Lin and Nansteel (1987), and Tong and Koster (1993).

There exist relatively few studies concerning transient natural convection of cold water in vertical rectangular enclosures. The transient natural convection cooling of cold water in a rectangular enclosure was studied numerically by Vasseur and Robillard (1980) and Robillard and Vasseur (1981, 1982). Braga and Viskanta (1992) undertook a combined experimental and numerical investigation of the transient natural convection cooling of cold water by a vertical cold wall at 0°C of a vertical rectangular enclosure of aspect ratio 0.5 with a free surface. The hot vertical wall temperature was equal to the initial temperature of stagnant water in the enclosure, which was varied from 8 to 20°C. Results presented were rather limited to the first 30 minutes of the transient cooling process inside the enclosure. A similar transient cooling problem but in a vertical enclosure of aspect ratio 0.75 was further studied by McDonough and Faghri (1994). The transient cooling processes considered were all found to reach steady state. The effect of density inversion on flow pattern and temperature distribution was found dominant with the initial and hot wall temperature above the density maximum temperature. Tong and Koster (1994) performed a numerical study of the transient natural convection of cold water in a vertical rectangular enclosure to examine the effect of aspect ratio in the range from 0.25 to 10.

From the foregoing studies concerning steady state or transient natural convection of cold water in vertical rectangular enclosures, it can be noticed that the Rayleigh numbers considered were rather restricted to those of below 10^6. For natural convection of cold water in vertical rectangular enclosures at high Rayleigh numbers ($Ra > 10^6$) there exists only three previous studies. Lankford and Bejan (1986) reported an experimental study of steady natural convection of cold water in a tall vertical enclosure of aspect ratio 5.05 for a Rayleigh number range of 10^8 to 10^{11}. The enclosure was differentially heated with mixed boundary conditions having a constant heat flux boundary for one vertical wall while an isothermal temperature below 4°C for the opposite vertical wall. When temperature of the hot and cold vertical walls encompassed the density maximum temperature, bicellular flow structure was observed to

prevail in the enclosure. On the other hand, Ivey and Hamblin (1989) performed experiments for natural convection of cold water in a differentially heated shallow enclosure of aspect ratio in the range between 0.1 to 0.5 with the Rayleigh numbers varying between 10^5 and 10^8. The vertical walls were maintained isothermal, respectively, at 0°C and 8°C. Similar to the finding for the tall enclosure by Lankford and Bejan (1986), the buoyant flow field of cold water in the low-aspect-ratio enclosure featured a bicellular structure. Moreover, they observed through the dye-injection flow visualization that the interior sinking jet-like flow structure along the maximum density contour was unstable for $Ra_H > 10^7$. Recently, by means of a finite element method, Nishimura *et al.* (1995) attempted to simulate natural convection flow of cold water in a vertical enclosure of aspect ratio 1.25 at high Rayleigh numbers of $10^5 \sim 10^8$. However, the numerically predicted flow and temperature fields of cold water at the high Rayleigh numbers, that may be expected to be unstable, remained stable displaying a symmetry with respect to the midline of the enclosure. The adoption of a symmetric correlation for the density of water as a function of temperature in their numerical calculations was attributed to the failure of yielding unstable flows at the high Rayleigh numbers. Asymmetries of flow pattern and temperature profile as the requisites for the onset of unstable cold water convection in the enclosure were suggested.

A reflection through the foregoing literature reveals that there appears no previous study, to our best knowledge, concerning the transition behavior of natural convection in vertical rectangular enclosure containing cold water. The present study therefore aims to explore the transition from steady to unsteady natural convection in a vertical rectangular cold-water-filled enclosure with an aspect ratio of eight. The physical configuration considered here is primarily motivated by the problem of related interest concerning natural convection dominated melting of ice in a rectangular enclosure (Ho and Chu, 1993; Ho *et al.*, 1996). Moreover, in an earlier study (Ho and Lin, 1990) concerning natural convection of cold water in the vertical annuli, a somewhat unstable multicellular flow structure featuring a wavy maximum density contour was found in an aspect-ratio-eight annulus. It was then quite natural for us to further continue with this particular aspect ratio. To this end, direct numerical simulations have been undertaken to obtain the long-time behavior of the two-dimensional natural convection of cold water in the tall vertical rectangular enclosure.

Problem formulation

Consider a two-dimensional rectangular enclosure of height H and width W filled with water near its density extreme (cold water) as illustrated in Figure 1. The left and right vertical walls of the enclosure are differentially heated at constant uniform temperature T_h and T_c ($< T_h$), respectively. The horizontal sidewalls of the enclosure are assumed adiabatic. The Boussinesq approximation is assumed to be valid for the two-dimensional buoyancy-driven flow of cold water within the enclosure. Moreover, the nonlinear density-

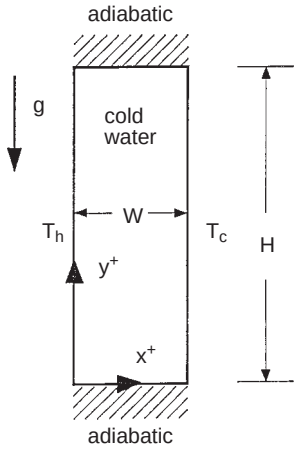

Figure 1.
Schematic diagram of physical configuration and coordinate system

temperature relation of cold water is described incorporating a correlation proposed by Gebhart and Mollendorf (1974) of the following form:

$$\rho = \rho_m(1 - rsp \cdot |T - T_m|^b) \qquad 0^\circ\mathrm{C} \le T \le 20^\circ\mathrm{C} \tag{1}$$

where ρ_m (=999.972kg/m^3 is the maximum density, $rsp = 9.297173 \times 10^{-6}$ $(^\circ\mathrm{C})^{-b}$, $T_m = 4.0293^\circ\mathrm{C}$ and $b = 1.894816$.

The dimensionless equations governing the time-dependent buoyancy-driven flow of cold water may be written in terms of vorticity, stream function and temperature as

$$\left.\begin{aligned} \frac{\partial\omega}{\partial\tau} + u\frac{\partial\omega}{\partial x} + v\frac{\partial\omega}{\partial y} &= Pr\left[\frac{\partial^2\omega}{\partial x^2} + \frac{\partial^2\omega}{\partial y^2}\right] - PrRa_W\frac{\partial|\theta-\theta_m|^b}{\partial x} \\ \frac{\partial^2\psi}{\partial x^2} + \frac{\partial^2\psi}{\partial y^2} &= -\omega \\ \frac{\partial\theta}{\partial\tau} + u\frac{\partial\theta}{\partial x} + v\frac{\partial\theta}{\partial y} &= \frac{\partial^2\theta}{\partial x^2} + \frac{\partial^2\theta}{\partial y^2} \end{aligned}\right\} \tag{2}$$

where ω, ψ, and θ are the dimensionless vorticity, stream function, and temperature, respectively. Moreover, τ, θ_m, Pr and Ra_W are the dimensionless time, the density inversion parameter, the Prandtl number, and the Rayleigh number, respectively.

The boundary conditions of the present problem are taken as

$$\left.\begin{aligned} \psi = u = v = 0, \quad x = 0,1, \quad y = 0,A, \\ \theta = 1, \quad x = 0, \\ \theta = 0, \quad x = 1, \\ \frac{\partial\theta}{\partial y} = 0, \quad y = 0,A. \end{aligned}\right\} \tag{3}$$

As the initial conditions, the solutions calculated earlier for a different Rayleigh number are taken. From the foregoing formulation, the present problem with

the aspect ratio A fixed at eight and the Prandtl number Pr = 12.5 for cold water apparently depends on two parameters: the Rayleigh number Ra_W and the density inversion parameter θ_m.

Moreover, the governing equation describing the conservation of dimensionless fluctuating kinetic energy, $(u_i' u_i'/2)$ (Janssen and Henkes, 1995) of oscillatory convection in the enclosure can be derived as the following form:

$$\frac{\partial}{\partial \tau}\left(\frac{u_i' u_i'}{2}\right) = \underbrace{-\frac{\partial}{\partial x_j}\left(u_i' \bar{u}_j \bar{u}_i + \bar{u}_j u_i' u_j'/2 + u_j' P + Pr\ u_i' \frac{\partial \bar{u}_i}{\partial x_j}\right)}_{\text{I}}$$

$$\underbrace{+\bar{u}_i \bar{u}_j \frac{\partial u_i'}{\partial x_j} - Pr \frac{\partial \bar{u}_i}{\partial x_j}\frac{\partial u_i'}{\partial x_j} + Pr\ Ra_W u_i' (\bar{\theta} - \theta_m)^2 \delta_{i2}}_{\text{II}} \tag{4}$$

$$\underbrace{-u_i' u_j' \frac{\partial \bar{u}_i}{\partial x_j} + Pr\ Ra_W [2(\bar{\theta} - \theta_m)\theta' + (\theta')^2]\delta_{i2} - Pr \frac{\partial u_i'}{\partial x_j}\frac{\partial u_i'}{\partial x_j}}_{\text{III}}$$

From close examination of equation (4), one may gain physical insight into the nature of the instability mechanism responsible for transition into unsteadiness. The first and second groups of terms (designated by I and II) on the right hand side of equation (4) become vanished by spatial integration over the enclosure and temporal integration over one period of oscillation, respectively. Only the third group of terms designated by III can contribute to the total fluctuating kinetic energy for an oscillatory convective flow in the enclosure. Specifically, the terms of $-u_i' u_j' \partial \bar{u}_i/\partial x_j$ and $Ra_w Pr[2(\bar{\theta} - \theta_m)\theta' + (\theta')^2]\delta_{i2}$ represent the local production of fluctuating kinetic energy due to the shear of the mean flow and the buoyancy force, respectively; while the term $-Pr\partial u_i'/\partial x_j \partial u_i'/\partial x_j$ represents the viscous dissipation of fluctuating kinetic energy. It should be noted that for mathematical simplicity in deriving equation (4), a parabolic form of density-temperature relation suggested by Simmons (1980) was adopted instead of using equation (1) directly.

Numerical method

The governing differential equations, equation (2), are discretized spatially with a finite difference method involving the second-order central-difference scheme for the diffusion terms and the QUICK-2D scheme (Leonard, 1983) for the convective terms. The integration of the equations in time is then performed fully explicitly with second-order accuracy. Boundary vorticity is treated using Thom formula (Roache, 1976).

In order to accurately resolve the high-gradient in the boundary layers developed along the vertical walls, a non-uniform grid in the x-direction, providing finer grids toward the vertical walls of the enclosure is constructed. A uniform grid is employed in the y-direction.

Each simulation is started using the results of previously obtained solution of nearby value of the Rayleigh number as the initial condition. At each time step, the discretized stream function equations are iteratively solved by a line successive relaxation method until a relative convergence criterion of less than 5×10^{-8} is met. The solution is considered to be converged to steady state if the relative convergence criteria of 10^{-7} and 10^{-8} are, respectively, satisfied for solutions of vorticity and temperature.

For stable and accurate explicit double-precision calculations on a DEC Alpha-Station 250/4/233, a time step of the order of 10^{-6} was found to be sufficiently small. It insures that at least 2,000 time increments were used to resolve the fine temporal scale of oscillatory convection flow for one period. Typical CPU time required for a simulation of oscillatory convection was approximately more than 120 hours. Grid resolution independence is assured by comparing solutions obtained on various gird systems ranging from 27×161 to 57×281 meshes. For instance, at $Ra_W = 10^6$ and $\theta_m = 0.4$ it was found that in comparison with that using the finer mesh, 37×201 mesh can yield a difference of less than 0.8 per cent, 0.6 per cent and 1.2 per cent, respectively, for the dimensionless oscillation frequency f, $\bar{\psi}_{\max}$ and $\bar{\psi}_{\min}$. Accordingly, in the present study a grid system of 37×201 was used for the simulations of the Rayleigh numbers up to 10^6, while a finer mesh of 47×241 was employed for those beyond 10^6.

Furthermore, accuracy of the present numerical code has been established through a series of validation simulations. Simulations for two-dimensional natural convection in an air-filled square enclosure have been performed and were found to agree well with the results presented by Le Quéré (1991) and de Vahl Davis and Jones (1983), as demonstrated in Table I. Further validation simulations have been conducted for the problem of transient natural convection of cold water in a vertical rectangular enclosure of $A = 1.25$ considered by Nishimura *et al.* (1995). The calculated results of the surface-averaged Nusselt number at four different values of T_h (= 4, 6, 8, and 10°C) with $T_c = 0$ °C were found to agree both qualitatively and quantitatively well with those of Nishimura *et al.* (1995). Meanwhile, similar to the findings of Nishimura *et al.* (1995) and Ivey and Hamblin (1989), the steady state was found to be approached in time of $2t_f$, where t_f is a time scale of $HW(2\alpha Ra_H^{1/4})$ with $Ra_H = g \cdot rsp\Delta T^b H^3/\nu\alpha$.

Table I. Comparison of results for natural convection in air-filled square enclosure

	$(\overline{Nu}_h, \psi_{\max}, f_d)$		
Ra_W	de Vahl Davis and Jones (1983)	Le Quéré (1991)	Present simulation
10^5	(4.509, –, –)	(4.522, 9.619, –)	(4.540, 9.607, –)
10^6	(8.817, 16.75, -)	(8.825, 16.811, –)	(8.850, 16.825, 0.097)
10^7	(–, –, –)	(16.523, 30.170, –)	(16.685, 30.244, 0.095)
10^8	(–, –, –)	(30.225, 53.85, 0.107)	(30.770, 54.452, 0.101)

Results and discussion

The numerical simulations were performed by varying Rayleigh number at two values of the density inversion parameter θ_m = 0.4 and 0.5, where the density inversion effects may affect most significantly on the buoyant flow (Seki *et al.*, 1978; Lin and Nansteel, 1978). The numerical results are described hereinafter to unveil the prominent effects of increasing the Rayleigh number progressively under a fixed θ_m on the transient evolution to steadiness and the onset of transition into unsteadiness of the buoyancy-driven flow in the enclosure. The flow structure and the temperature distribution are respectively illustrated by the contour plots of streamlines and isotherms. The contours of solid and dashed lines in the plots represent, respectively, the positive and negative values of the physical quantity of interest. Also superimposed on the contour maps is the maximum density contour of cold water denoted by the heavy dashed line.

Transient to steady convection

The simulations for θ_m= 0.4 begin with $Ra_W = 7 \times 10^4$ using a stagnant water at a uniform temperature of $\theta = 0$ as the initial conditions. Development of the natural convection of cold water within the enclosure was initiated by suddenly raising the temperature of the left vertical wall to a constant value $\theta = 1$. The time-dependent solution was found to evolve asymptotically toward a steady state flow field and temperature distribution shown in Figure 2(a). A contra-rotating bicellular flow structure dominated by the clockwise circulation prevails in the enclosure. The isotherms are nearly parallel in the enclosure, except for the bottom and the upper quarter regions, in which a convection-dominated distribution of isotherms can be discerned. In particular, similar to what was observed in the experiment of Lankford and Bejan (1986), the flow structure along the maximum density contour may be viewed as a sinking maximum density jet emanating from the upper part of the cold wall. The maximum density jet-like stream slants downward and then turns into the enclosure core through a "neck-down" region of the clockwise circulation flow.

Simulations for θ_m = 0.4 were then continued for the subsequently higher Rayleigh numbers using the solution for the closest lower Rayleigh number as the initial condition. With the increase of Rayleigh number up to 4×10^5, the oscillatory transient flow developments in these cases all were found to evolve ultimately toward steady state, but at increasingly longer time with the increase in the Rayleigh number. This is a clear indication of approaching critical point of transition into unsteadiness. At $Ra_W = 4 \times 10^5$, for instance, the steady state flow structure and temperature distribution, as displayed in Figure 2(b), is reached after $\tau > 4.0$. As can be noticed in the streamline plot of Figure 2(b), with the increasing Ra_W, the contra-rotating bicellular flow is greatly strengthened and is meanwhile superimposed by a multicellular structure within the clockwise circulation. This signifies the onset of transition

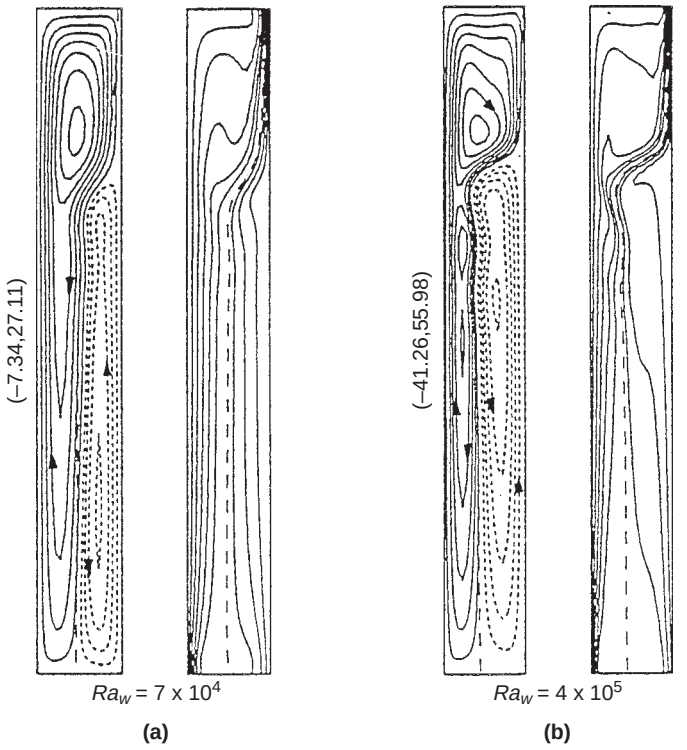

Figure 2.
Steady state results of streamline pattern (left) and isotherm distribution (right) for $\theta_m = 0.4$;
(a) $Ra_W = 7 \times 10^4$ and
(b) $Ra_W = 4 \times 10^5$

from unicellular to multicellular regime. Waviness of the thermal boundary layer along the hot wall as well as of the maximum density contour is visible around the neck-down region.

Similar to those for $\theta_m = 0.4$, the time-dependent simulations under the condition of $\theta_m = 0.5$ start with $Ra_W = 3 \times 10^4$ using an initial condition of stagnant cold water at a temperature of $\theta = 0$. The simulation approaches a steady state featuring a rather symmetric flow structure of two contra-rotating circulation regions of approximately equal strength and size demarcated by the vertically oriented maximum density contour (not shown here). Up until $Ra_W = 7 \times 10^4$ the steady state natural convection persists for the subsequent simulations based on the solution for the previously lower Rayleigh number.

Transition to oscillatory convection

As the Rayleigh number is further increased to 5×10^5 under the condition of $\theta_m = 0.4$, the transient flow development in the enclosure reaches a regime of self-sustained periodic oscillation in time, as illustrated in Figure 3. The buoyancy-driven flow of cold water in the enclosure has evolved from a steady state to a periodic attractor through a Hopf bifurcation. It can be noticed from Figures 3(d) and 3(e) that the oscillation amplitude of the stream function at the

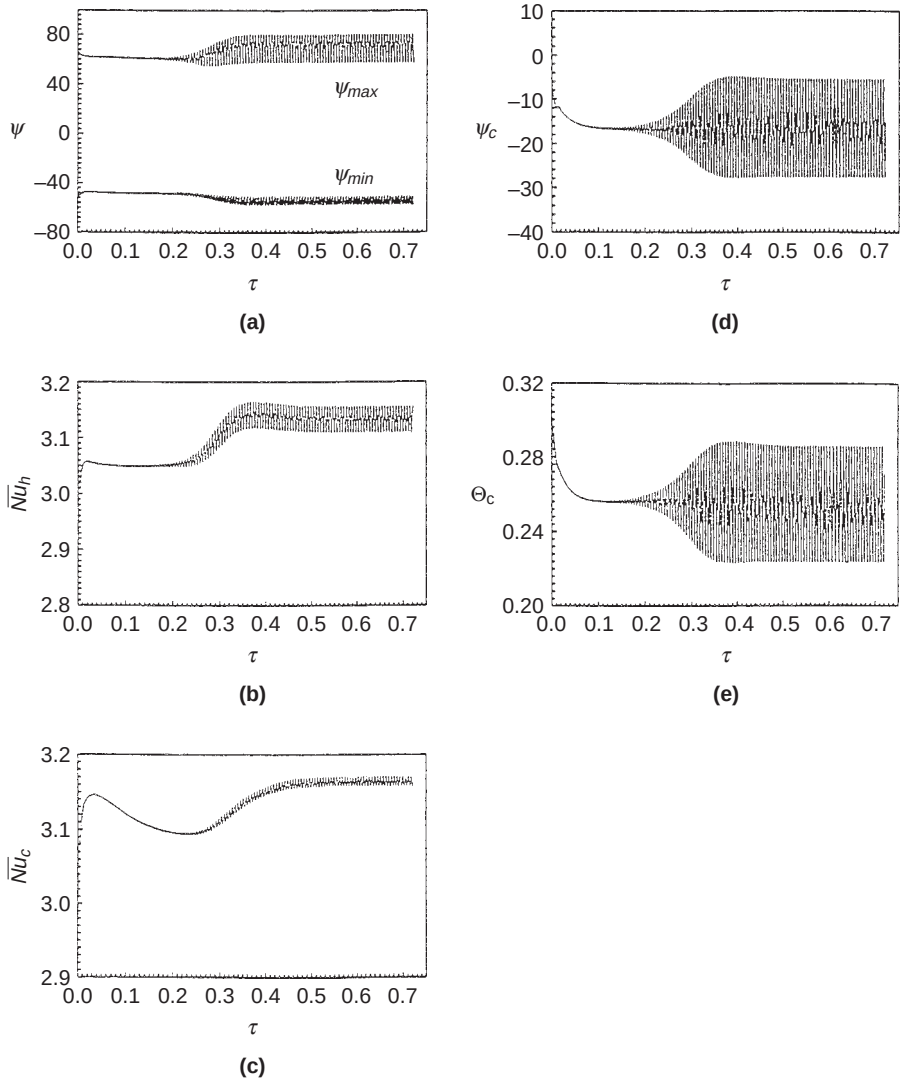

Figure 3.
Time histories of (a) ($\psi_{\max}$, $\psi_{\min}$), (b) $\overline{Nu}_h$, (c) $\overline{Nu}_c$, (d) ψ_c, and (e) θ_c for $Ra_W = 5 \times 10^5$ and $\theta_m = 0.4$

center point, ψ_c, is considerably larger than that of the corresponding temperature θ_c. The Fourier spectrum for the periodic variation of the five quantities shown in Figure 3 (not shown here) reveals that all of them are impelled at the same dimensionless frequency of $f = 166.67$. Figure 4 displays a time sequence of the flow structure and temperature distribution over one period of oscillation at $Ra_W = 5 \times 10^5$. A cyclic sequence of splitting and merging of the upward-drifting secondary vortices within the contra-rotating double-circulation structure can be clearly observed from the streamline plots of Figure 4. As a result, the jet-like flow along the maximum density contour

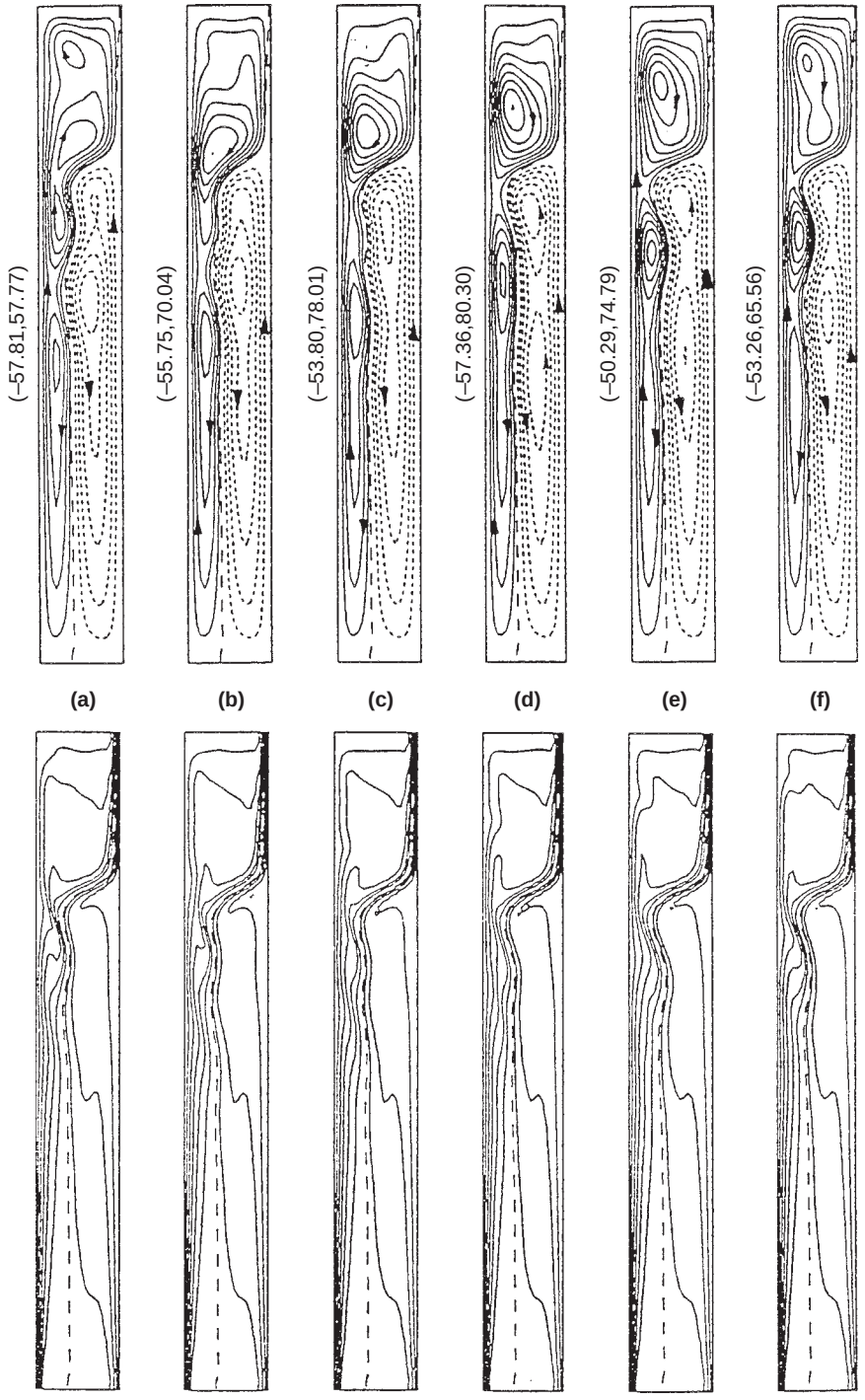

Figure 4.
Cyclic variation of streamlines (upper) with $\Delta\psi = 10$ and isotherms (lower) with $\Delta\theta = 0.1$ for $Ra_W = 5 \times 10^5$ and $\theta_m = 0.4$

displays a traveling wave motion as it turns through the neck-down region into the core of the enclosure. Similar wavy sinking jet flow structure has been experimentally visualized by Lankford and Bejan (1986) in a cold-water-filled enclosure of aspect ratio 5.05 subjected to the mixed thermal boundary conditions on the vertical walls. In addition, in accordance with the upward-drifting movement of the clockwise secondary vortices through the region, a cyclic variation of wavy isotherms in the thermal boundary layer can be discerned along the hot wall. Conversely, near the bottom quarter region of the enclosure the maximum density contour remains essentially stagnant, where a rather isothermal region exists.

To gain further insight of the space-time structure of the oscillatory convection, the instantaneous fluctuating stream function and temperature fields at the instants corresponding to those shown in Figure 4 over an oscillation period are presented in Figure 5. The fluctuating value of the stream function or temperature was evaluated in every grid point by subtracting the local time-averaged value from the local instantaneous value. The solid and dashed contours in Figure 5 denote, respectively, the local instantaneous value higher and lower than the local time-averaged value. Two numbers enclosed in the parentheses, shown with each fluctuation contour plots, are, respectively, the maximum and minimum magnitudes of the fluctuating quantities. The contour plots of fluctuating stream function and temperature clearly display a cyclic sequence of initiation, growth, upward movement, and decay. From the fluctuating stream-function plots, one can notice that the flow velocity fluctuation displays a form of consecutive structure with alternate sign of magnitude. The velocity fluctuation starts at a location below the mid-height, $y \cong 0.36$, of the enclosure; and then grows in amplitude as it moves upward along the maximum density contour. Peak amplitude of the fluctuation appears around the neck-down region. Afterwards, as it further drifts upward past the neck-down region into the upper-quarter portion of the enclosure, the velocity fluctuation starts to decay with its center shifting toward the hot wall. This appears to be synchronized with the cyclic movement displayed by the clockwise secondary vortex center that is shown in Figure 4. On the other hand, unlike the stream function fluctuations, the temperature fluctuations appear to be mostly confined within the clockwise multicellular region next to the hot wall. The consecutive locally hot and cold patterns shown by the fluctuating temperature contours in Figure 5 undergo a somewhat different cyclic evolution than that of the corresponding fluctuating stream function. Starting from a location below mid-height of the thermal boundary layer along the hot wall, the fluctuating temperature structure arises and then grows in magnitude as it is drifted upward by the vertical boundary layer flow. A close look at the temperature fluctuation contours reveals that the growing temperature fluctuation penetrates across the maximum density contour, where it is subjected to downward dragging by the sinking maximum density jet-like flow. As a result, the temperature fluctuation structure beyond mid-height of the hot wall is seen to split into a twin-peak structure with one of the fluctuation

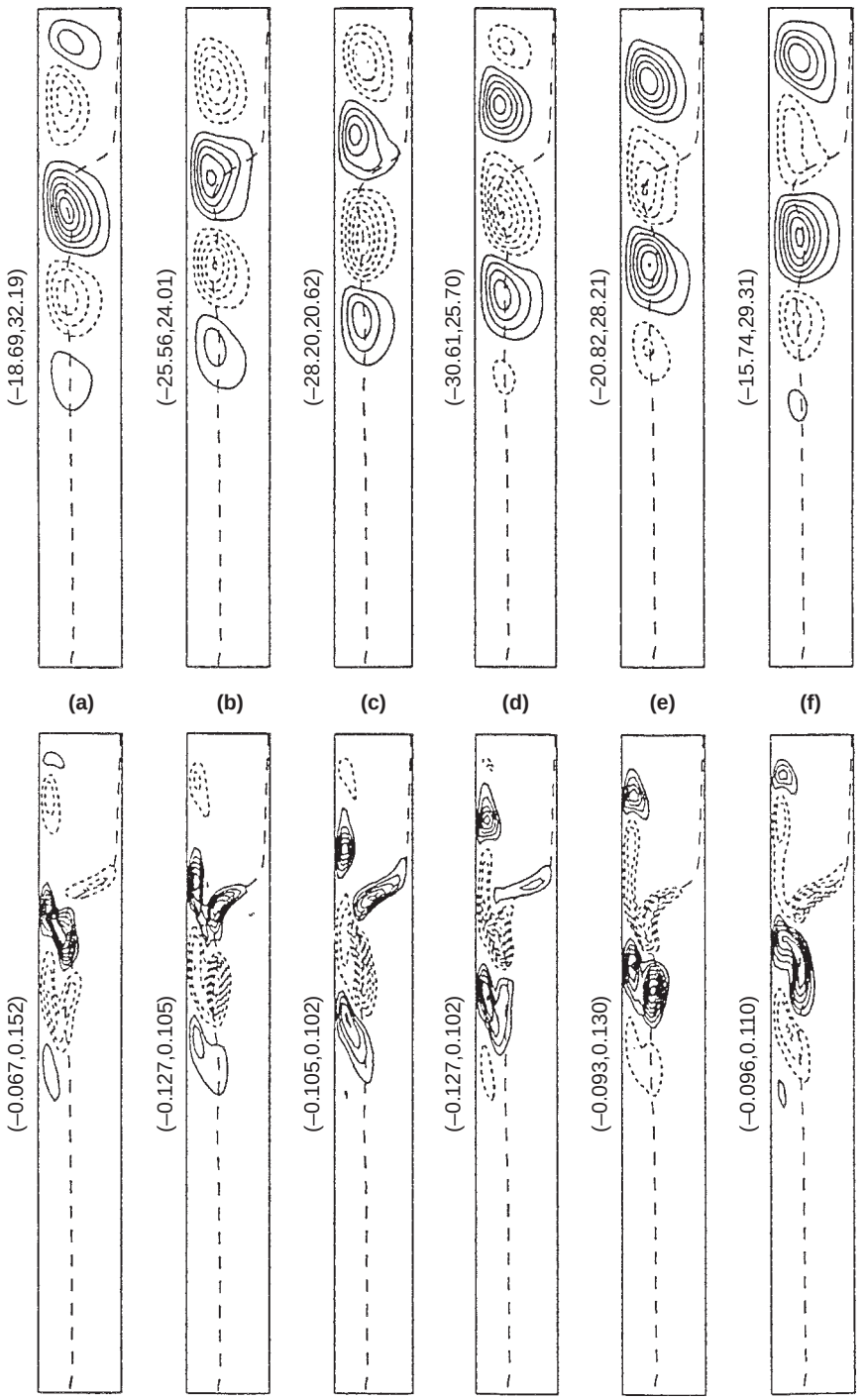

Figure 5.
Cyclic sequence of the fluctuating stream function (upper) and temperature (lower) fields for $Ra_W = 5 \times 10^5$ and $\theta_m = 0.4$ at the time instants corresponding to those in Figure 4

peaks centered on the maximum density contour. The twin-peak fluctuation structure of temperature reaches its maximum magnitude around the neck-down region. This is also where the waviness in isotherms and the maximum density contour can be clearly detected. Afterwards, the twin-peak fluctuation structure begins to decay in magnitude and gradually separates into two isolated structures while it passes through the neck-down region. One of the separated temperature fluctuation structures then moves along the upward-slanted maximum density contour and eventually diminishes at the cold wall. Meanwhile, the other separated fluctuation structure continues to be convected upward and diminishes at the ceiling of the enclosure.

Further insight into the nature of the instability mechanism for the present case can be gained by examining the production terms of the fluctuating kinetic energy of the oscillatory convection in the enclosure. That is the term group III of equation (4), which may be due to the flow shear and/or the buoyancy force. To this end, equation (4) is integrated over one period of the oscillation of the present case. The resultant distributions of local production of time-integrated fluctuating kinetic energy due to flow shear and buoyancy are presented in Figure 6, respectively. The shear-induced positive fluctuating kinetic energy, as shown in Figure 6(a), only exists on either side of the maximum density contour in the neck-down region. This shear-induced instability, however, is not as dominant as the positive production region due to buoyancy displayed in

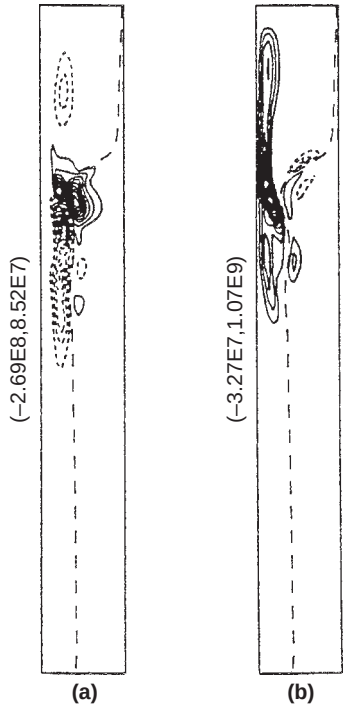

Figure 6.
Spatial distribution of local production of time-integrated fluctuating kinetic energy due to (a) flow shear and (b) buoyancy for $Ra_W = 5 \times 10^5$ and $\theta_m = 0.4$. Negative iso-values are denoted by dotted lines

Figure 6(b). The positive buoyancy-induced production is present mostly in the second half of the vertical boundary layer along the hot wall and appears to be largest around the neck-down region. On the other hand, in the counter-clockwise circulation region a relatively small contribution to the buoyancy-induced production can be detected along the wavy maximum density contour. It can then be concluded from Figure 6 that the buoyancy or the temperature fluctuation is the primary source for local production of the fluctuating kinetic energy. This can be further confirmed by checking the total fluctuating kinetic energy production budget, which is obtained by integrating the local production of fluctuating kinetic energy shown in Figure 6 over the entire enclosure. The result reveals that for the present case the production of total fluctuating kinetic energy is contributed completely by the buoyancy; while the flow shear contributes negatively (–9.7 percent) to the production of total fluctuating kinetic energy. This clearly indicates that the transition from steady into periodically oscillatory convection of cold water in the enclosure at $\theta_m = 0.4$ is a buoyancy-driven instability.

Supercritical simulations for $\theta_m = 0.4$ were further conducted by progressive increase of the Rayleigh number up to 2×10^6. The solutions to these cases all remain periodic with increasingly higher frequencies f. Moreover, the critical Rayleigh number for the transition into oscillatory convection under $\theta_m = 0.4$, based on these simulations, is estimated to be $4 \times 10^5 < (Ra_W)_{cr} \leq 5 \times 10^5$ (or $2.05 \times 10^8 < (Ra_H)_{cr} \leq 2.56 \times 10^8$).

Next, for $\theta_m = 0.5$ the oscillatory convection in the enclosure was first observed at $Ra_W = 8 \times 10^4$ with a frequency of $f = 41.32$, which is much lower than the value of 166.67 found for $Ra_W = 5 \times 15^5$ at $\theta_m = 0.4$. Figure 7 displays the cyclic sequence of the stream function and temperature fields at $Ra_W = 8 \times 10^4$. The flow structure shown in Figure 7 features a somewhat similar cyclic sequence of unsteady multicellular flow development to that found at $\theta_m = 0.4$. That includes onset at the bottom region, upward drifting, growth, and decay of the split vortices within the contra-rotating double-circulation flows of approximately equal size, respectively. Consequently, the maximum density contour becomes corrugated featuring an upward traveling sinusoidal wave through the core region of the enclosure. The wavelength of the traveling wave of the maximum density contour, which is also the distance between the co-rotating upward-drifting secondary vortices, tends to increase while propagating upward and has an averaged dimensionless value of $\lambda/H = 0.226$. Furthermore, it can be seen that the maximum density jet flow coming off the midpoint of the ceiling turns unstable, undergoing a series of horizontal meanders in a diminishing magnitude while sinking through the central core region of the enclosure. It should be noted that for the present case the Rayleigh number based on the enclosure height Ra_H ($= 4.10 \times 10^7$) appears to satisfy the estimated criterion of $Ra_H > 10^7$ by Ivey and Hamblin (1989). Moreover, the isotherms within the contra-rotating circulation regions (shown in Figure 7) exhibit a cyclic sequence of upward traveling wave trains emanating at the

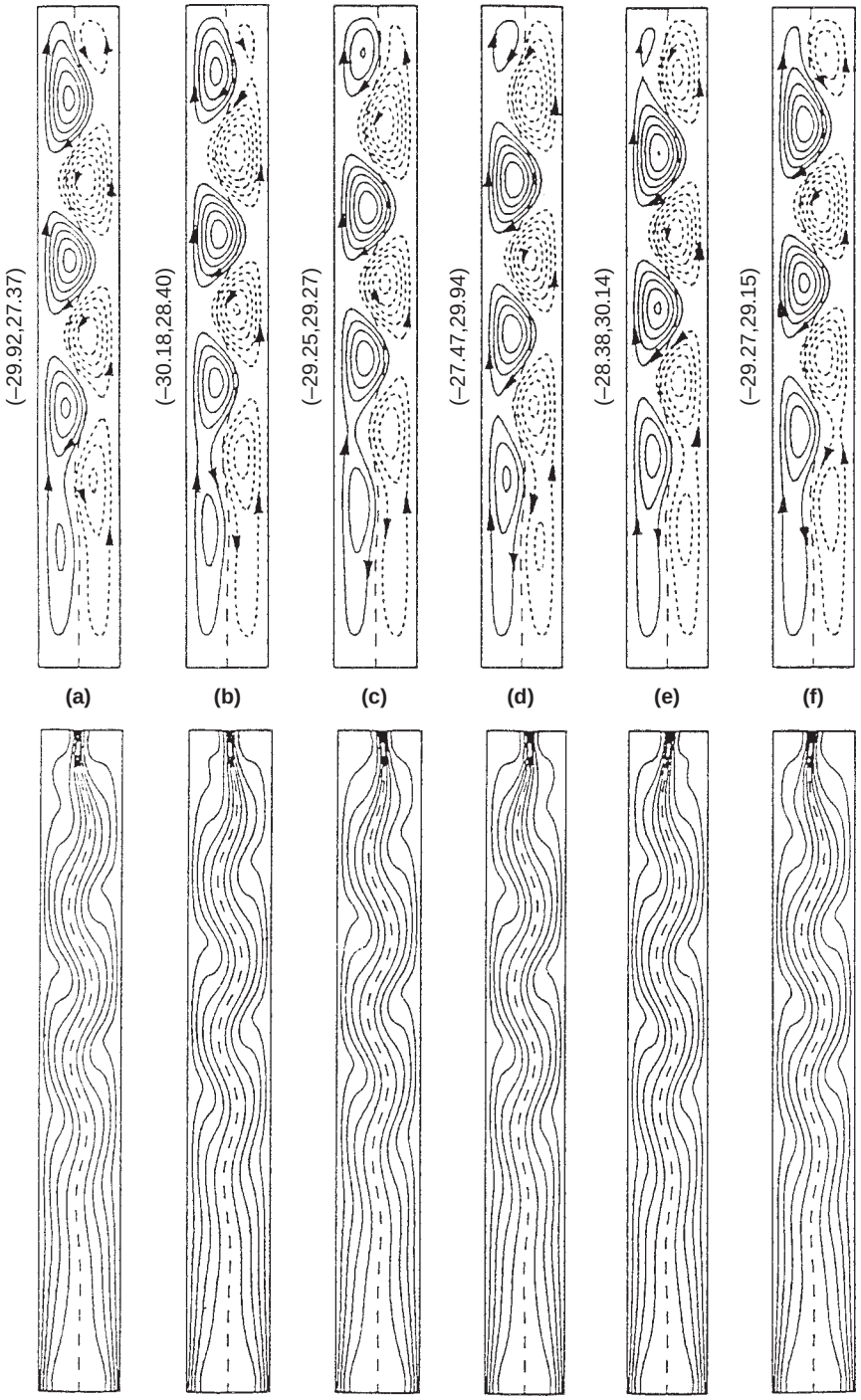

Figure 7.
Cyclic variation of streamlines (upper) with $\Delta\psi = 5$ and isotherms (lower) with $\Delta\theta = 0.1$ for $Ra_W = 8 \times 10^4$ and $\theta_m = 0.5$

bottom quarter-height of the vertical walls. This cyclic variation appears to be in synchronization with the traveling sinusoidal wave motion of the maximum density contour.

The space-time structures of the stream function and temperature fields display more or less symmetry with respect to the wavy maximum density contour. Accordingly, a symmetric time-averaged flow and temperature structure in the enclosure as shown in Figure 8 results. A co-rotating bicellular flow structure can be seen to be superimposed on, respectively, the clockwise and counter-clockwise circulation flows of approximately equal strength, which are demarcated by a centrally-located, vertically oriented maximum density contour. Another interesting fact which can be observed in Figure 8 is that the time-averaged isotherms within the contra-rotating double-circulation regions feature a conduction-regime distribution with no vertical temperature stratification in their respective core regions. Under this circumstance, the internal wave motion is virtually precluded from taking place inside the cold-water-filled enclosure. This means that the sinusoidal waviness of the maximum density jet-like flow structure is simply caused by the onset of unstable co-rotating multicellular secondary vortices within the contra-rotating bicellular flow regions.

In Figure 9 the cyclic spatial structure of the fluctuating stream function and temperature for $Ra_W = 8 \times 10^4$ are presented. Both fluctuating quantities

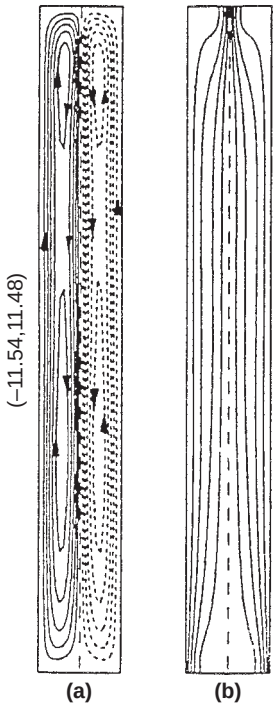

Figure 8.
Periodically time-averaged structures of (a) flow and (b) temperature fields for $Ra_W = 8 \times 10^4$ and $\theta_m = 0.5$

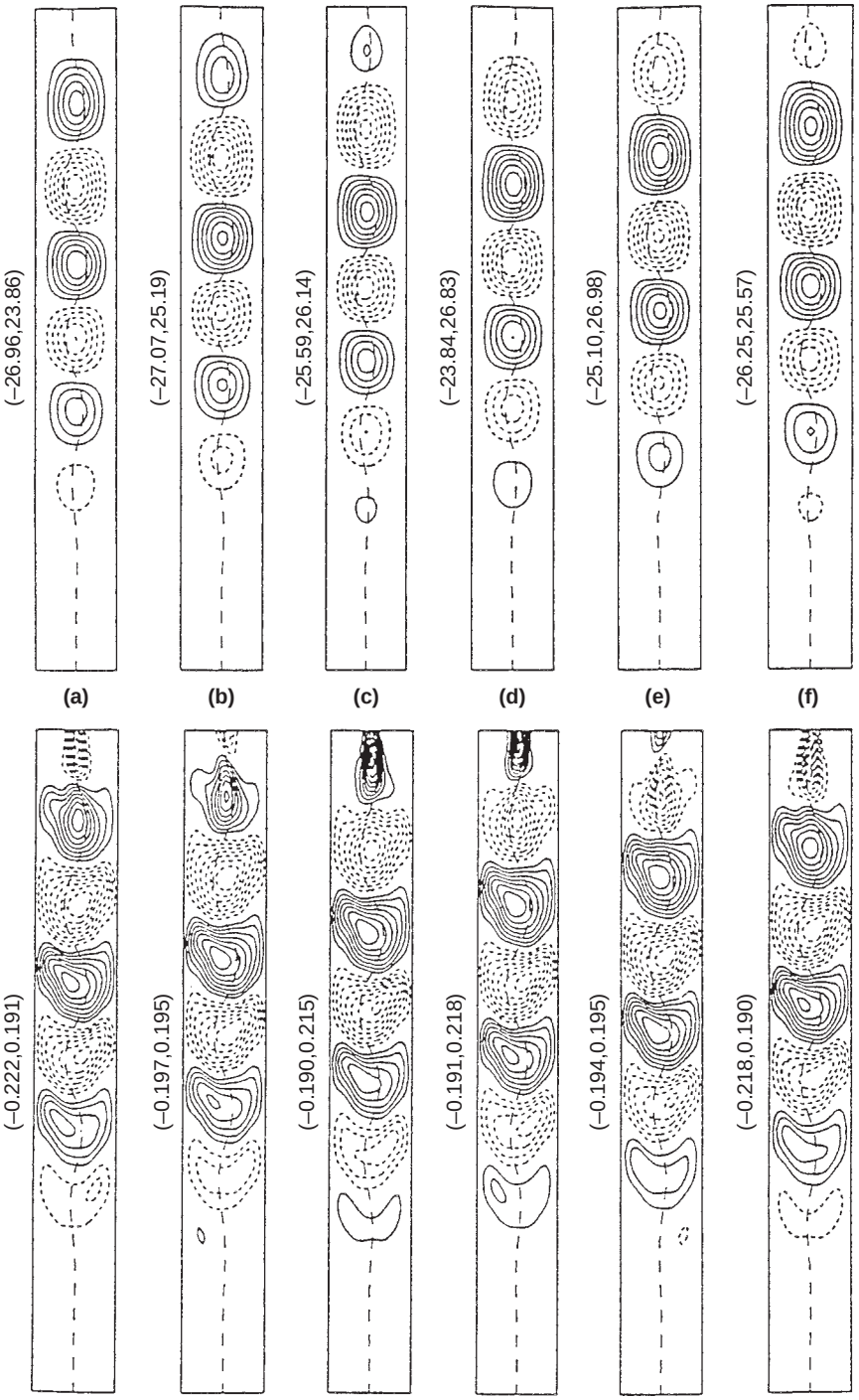

Figure 9.
Cyclic sequence of the fluctuating stream function (upper) and temperature (lower) fields for $Ra_W = 8 \times 10^4$ and $\theta_m = 0.5$

undergo a similar cyclic variation. The fluctuation arises at the bottom region, whereupon the maximum density contour starts it meandering; and then grows in size and magnitude on its course of upward drifting along the vertical mid-line of the enclosure. Finally, the fluctuation diminishes at the ceiling of the enclosure. A closer examination of the fluctuation structures reveals that the consecutive fluctuation structures of alternate sign penetrate extensively across the enclosure and have their peaks always centered to the left or the right side of the wavy maximum density contour. Moreover, the spatial distributions of local production of the time-averaged fluctuating kinetic energy due to flow shear and buoyancy are, respectively plotted (as shown in Figure 10) to further identify the nature of the instability mechanism. The local production of time-integrated fluctuating kinetic energy due to buoyancy or shear exhibits a symmetric distribution with respect to the time-averaged maximum density contour. It is evident from Figure 10 that the buoyancy is the dominant source for the fluctuating kinetic energy production with a spatial distribution occupying nearly the whole upper half portion of the enclosure. The flow shear only contributes energy to the fluctuating flow around the upper quarter portion of the maximum density contour. Further, the total production of the fluctuating kinetic energy in the enclosure is found to be similar to that found for $\theta_m = 0.4$, solely contributed by the buoyancy. The

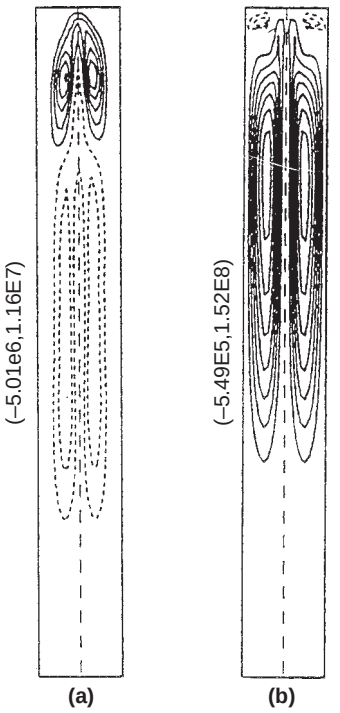

Figure 10.
Spatial distribution of local production of time-integrated fluctuating kinetic energy due to (a) flow shear and (b) buoyancy for $Ra_W = 8 \times 10^4$ and $\theta_m = 0.5$. Negative iso-values are denoted by dotted lines

supercritical Hopf bifurcation to oscillatory convection of cold water in the enclosure under $\theta_m = 0.5$ is therefore of thermal in nature associated with the temperature fluctuation.

As the Rayleigh number is further increased progressively up to 10^5 for $\theta_m = 0.5$, the buoyant flow in the cold-water-filled enclosure remains oscillatory in time. The critical Rayleigh number $(Ra_W)_{cr}$ for $\theta_m = 0.5$ may be bounded to the range between 7×10^4 and 8×10^4 (or $3.584 \times 10^7 < (Ra_H)_{cr} < 4.10 \times 10^7$). This critical Rayleigh number appears to be much smaller than that found for $\theta_m = 0.4$.

This clearly reflects the significant role played by the density inversion parameter θ_m, which primarily determines the position or profile of the maximum density contour, on the transition into unsteadiness of nature convection in the cold-water-filled enclosure.

Heat transfer results

Finally, results of the surface-averaged heat transfer rate for the steady state or periodically oscillatory convection of cold water in the enclosure are presented by a time- and surface-averaged Nusselt number along the hot wall, $\overline{Nu}_{h,m}$.

In Figure 11, the data of $\overline{Nu}_{h,m}$ are related to the Rayleigh number for the two values of θ_m considered here and can be correlated as

$$\overline{Nu}_{h,m} = CRa_W^n \tag{5}$$

where the coefficient C and the exponent n are evaluated by means of the least-squares regression for the two values of θ_m as listed in Table II. The small exponent value of 0.124 for the steady state natural convection at $\theta_m = 0.5$ is another indication of convective flow in the conduction regime of natural convection heat transfer across the enclosure.

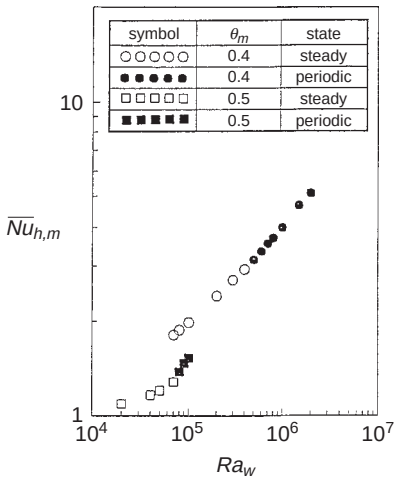

Figure 11.
Time- and surface-averaged heat transfer rates across the enclosure for $\theta_m = 0.4$ and 0.5

Further scrutiny of Figure 11 reveals that at a fixed Rayleigh number the heat transfer rate for $\theta_m = 0.5$ is smaller than that for $\theta_m = 0.4$. This finding is consistent with the well-known density-inversion effect on the nature convection heat transfer across the cold-water-filled enclosure.

Concluding remarks

This study is focused on the transition into oscillatory natural convection of cold water in a two-dimensional vertical rectangular enclosure with an aspect ratio of eight at two values of the density inversion parameter, $\theta_m = 0.4$ and 0.5. Through a series of numerical simulations, we have illustrated that with incremental increase in the Rayleigh number, the steady convective flow of cold water in the enclosure undergoes transition through a Hopf bifurcation, leading to a self-sustained periodically oscillatory regime.

The position or profile of the maximum density contour of cold water in the enclosure, which is primarily determined by the density inversion parameter, is found to have a significant effect on the time-dependent evolution of buoyancy-driven convective flow. Nature of the transitional instability into oscillatory convection of cold water is demonstrated to be buoyancy-driven for both values of θ_m considered. The thermally driven instability of natural convection in the cold water-filled enclosure is found to feature a transition from unicellular to periodically upward-drifting multicellular structure, respectively, within the contra-rotating bicellular flow regions. A traveling wave motion along the maximum density contour accordingly results. The critical Rayleigh number at $\theta_m = 0.4$ is found to be approximately one order of magnitude larger than that corresponding to $\theta_m = 0.5$.

As the final concluding remarks, we are fully aware that the assumption of two-dimensional flow in the present study precludes the effects of three-dimensionality on the onset of unsteadiness. It is, however, expected that the two-dimensional simulations can still reveal well the dynamic characteristics of transitional buoyant flow under the influence of density inversion. This has been supported from our preliminary results of direct three-dimensional simulations for the present configuration that are currently underway.

Results of the three-dimensional effects on the transition to unsteady convection of cold water in the tall rectangular enclosure will be presented in a future paper. Moreover, the influence of the aspect ratio of the enclosure and of the density inversion parameter in wider ranges certainly deserves further investigations.

Table II.
Coefficients and exponents of heat transfer correlation, equation (5), for $\theta_m = 0.4$ and 0.5

θ_m	C	n	Ra_W range	Averaged deviation
0.4	0.0574	0.307	$7 \times 10^4 \sim 2 \times 10^6$	1.3%
0.5	0.317	0.124	$2 \times 10^4 \sim 7 \times 10^4$	1.0%
	0.0046	0.506	$7 \times 10^4 \sim 10^5$	0.8%

References

Braga, S.L. and Viskanta, R. (1992), "Transient natural convection of water near its density extremum in a rectangular cavity", *Int. J. Heat Mass Transfer*, Vol. 35, pp. 861-75.

de Vahl Davis, G. and Jones, J.P. (1983), "Natural convection in a square cavity: a comparison exercise", *Int. J. Numer. Methods Fluids*, Vol. 3, pp. 227-48.

Gebhart, B. and Mollendorf, J. (1974), "A new density relation for pure and saline water", *Deep Sea Research*, Vol. 24, pp. 831-8.

Ho, C.J. and Chu, C.H. (1993), "The melting process of ice from a vertical wall with time-periodic temperature perturbation inside a rectangular enclosure", *Int. J. Heat Mass Transfer*, Vol. 36, pp. 3171-86.

Ho, C.J. and Lin, Y.H. (1990), "Natural convection of cold water in a vertical annulus with constant heat flux on the inner cylinder", *J. Heat Transfer*, Vol. 112, pp. 117-23.

Ho, C.J., Yang, S.L. and Chu, C.H. (1996), "Prediction of oscillatory convection during melting of ice in a vertical rectangular enclosure", in Lee, Y. and Hallett, W. (Eds), *Proceedings of the 5th Int. Symposium on Thermal Engineering and Science for Cold Regions*, pp. 225-30.

Inaba, H. and Fukuda, T. (1984a), "Natural convection in an inclined square cavity in regions of density inversion of water", *J. Fluid Mech.*, Vol. 142, pp. 363-81.

Inaba, H. and Fukuda, T. (1984b), "An experimental study of natural convection in an inclined rectangular cavity filled with water at its density extremum", *J. Heat Transfer*, Vol. 106, pp. 109-15.

Ivey, G.N. and Hamblin, P.F. (1989), "Convection near the temperature of maximum density for high Rayleigh number, low aspect ratio, rectangular cavities", *J. Heat Transfer*, Vol. 111, pp. 100-5.

Janssen, R.J.A. and Henkes, R.A.W.M. (1995), "Influence of Prandtl number on instability mechanisms and transition in a differentially heated square cavity", *J. Fluid Mech.*, Vol. 290, pp. 319-44

Lankford, K.E. and Bejan, A. (1986), "Natural convection in a vertical enclosure filled with water near 4°C", *J. Heat Transfer*, Vol. 108, pp. 755-63.

Leonard, B.P. (1983), "A convectively stable, third-order accurate finite difference method for steady two-dimensional flow and heat transfer", in Shih, T.M. (Ed.), *Numerical Properties and Methodologies in Heat Transfer Hemisphere*, Washington, DC, pp. 211-26.

Le Quéré, P. (1991), "Accurate solutions to the square thermally driven cavity at high Rayleigh number", *Computer Fluids*, Vol. 20, pp. 29-41.

Lin, D.S. and Nansteel, N.W. (1987), "Natural convection heat transfer in a square enclosure containing water near its density maximum", *Int. J. Heat Mass Transfer*, Vol. 30, pp. 2319-29.

McDonough, M.W. and Faghri, A. (1994), "Experimental and numerical analyses of the natural convection of water through its density maximum in a rectangular enclosure", *Int. J. Heat Mass Transfer*, Vol. 37, pp. 783-801.

Nishimura, T., Wake, A. and Fukumori, E. (1995), "Natural convection of water near the density extremum for a wide range of Rayleigh numbers", *Numerical Heat Transfer, Part A*, Vol. 27, pp. 433-49.

Roache, P.J. (1976), *Computational Fluid Dynamics*, Hermosa, Albuquerque, NM.

Robillard, L. and Vasseur, P. (1981), "Transient natural convection heat transfer of water with maximum density effect and supercooling", *J. Heat Transfer*, Vol. 103, pp. 528-34.

Robillard, L. and Vasseur, P. (1982), "Convective response of a mass of water near 4°C to a constant cooling rate applied on its boundaries", *J. Fluid Mech.*, Vol. 118, pp. 123-41.

Seki, N., Fukusako, S. and Inaba, H. (1978a), "Free convection heat transfer with density inversion in a confined rectangular vessel", *Warme Stoffubertrag*, Vol. 11, pp. 145-56.

Seki, N., Fukusako, S. and Inaba, H. (1978b), "Visual observation of nature convective flow in a narrow vertical cavity", *J. Fluid Mech.*, Vol. 84, pp. 695-704.

Simmons, T.J. (1980), "Circulation modes of lakes and inland seas", *Can. Bul. Fish. Aquatic Sci.*, Vol. 203, pp. 1-146.

Tong, W. and Koster, J. (1993), "Natural convection of water in a rectangular cavity including density inversion", *International Journal of Numerical Methods for Heat & Fluid Flow*, Vol. 14, pp. 366-75.

Tong, W. and Koster, J. (1994), "Density inversion effect on transient natural convection in a rectangular enclosure", *Int. J. Heat Mass Transfer*, Vol. 37, pp. 927-38.

Vasseur, P. and Robillard, L. (1980), "Transient natural convection heat transfer in a mass of water cooled through 4°C", *Int. J. Heat Mass Transfer*, Vol. 23, pp. 1195-205.

Watson, A. (1972), "The effect of the inversion temperature on the convection of water in an enclosed rectangular cavity", *Q. J. Mech. Appl. Math.*, Vol. 15, pp. 423-46.